EPJ Web of Conferences **140**, 03010 (2017) DOI: 10.1051/epjconf/201714003010
Powders & Grains 2017

Relaxation processes after instantaneous shear rate reversal in a dense granular flow

Eduardo Rojas[1], *Rodrigo* Soto[2,⋆], *Eric* Clement[3], *Martin* Trulsson[3], and *Bruno* Andreotti[3]

[1] *Departamento de Ingeniería Mecánica, Facultad de Ingeniería, Universidad de Antofagasta, Antofagasta, Chile.*
[2] *Departamento de Física, Facultad de Ciencias Físicas y Matemáticas, Universidad de Chile, Santiago, Chile.*
[3] *École Supérieure de Physique et de Chimie Industrielles (ESPCI), Paris, France.*

Abstract. A numerical model of granular material at different packing fractions and under steady shear is submitted to a sudden shear reversal. We monitor consequences of the strong density and shear rate spatio-temporal heterogeneities, on the constitutive relations. We show that the dynamics can be decomposed into two subsequent regimes spanning a time scale inversely proportional to the shear rate. In the first regime, a non-local constitutive relation is satisfied, hence accounting for the spatial heterogeneity of the fluidity parameter. However at later time, we find that the local $\mu(I)$ constitutive relation can be applied, in spite of the fact that the fluidity parameter remains heterogeneous.

1 Introduction

The understanding of dense granular flows received an important impulse by the discovery of the local rheology laws [1–3]. Dry granular media in avalanches or planar Couette geometries are standard benchmarks where the normal pressure P and shear stress τ can be measured and analysed separately. It was found that in hard grain systems, the normalized shear stress $\mu = \frac{\tau}{P}$ –which can be associated to an effective friction coefficient– depends only on the dimensionless inertial number $I = \frac{\dot{\gamma} d}{\sqrt{P/\rho_p}}$, for a flow of particles of diameter d and mass density ρ_p, and shear rate $\dot{\gamma}$. The relation $\mu(I)$, shown in Fig. 3(a), constitutes a local rheology relation [1–3]. At steady state, it is associated with a second relation: $\phi(I)$ expressing the decrease of packing fraction with the inertial number. The limit $I \to \pm 0$ yields the maximum packing fraction value ϕ^* depending on the microscopic granular details, particularly on the friction coefficients. It is important to keep in mind that the only true limit, where a solid phase would emerge as a real rigidity transition, is obtained for zero friction and is called the jamming point, sometimes called the random close packing limit [4]. Therefore, as we will see later, nothing prevents the observation, as a transient, of local packing fractions larger than ϕ^* as long as they remain smaller than the random close packing limit.

The local rheology picture was extended to non-planar geometries by assuming that stress and shear-rate tensors remain parallel with a proportionally constant associated to μ, with I computed from the invariants of the tensor [5]. Computer simulations of a rotating drum show that those tensors are indeed not parallel but still their invariants are related via the $\mu(I)$ rheology [6]. Simulations of a flow on an inclined plane have shown also a small but finite angular deviation when an objective analysis of the tensors is performed [7]. For non-homogeneous fields, non-local effects were observed either close to jamming [1, 8, 9] or in the vicinity of a shear band [10–12]. Different theoretical visions were proposed to model or interpret these features via fluidity parameters [9, 13–16].

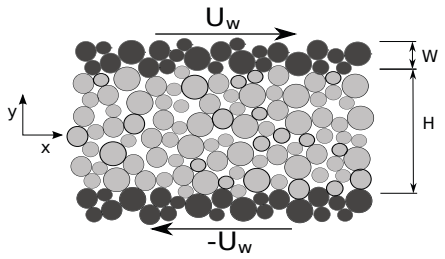

Figure 1. Set-up used in the simulations. The base width is $L = 45d$, the height is $H = 18d$, and the thickness of the confining walls is $W = 1.5d$.

In the application of the rheological laws to model flow regimes and hydrodynamic fields it is assumed that they would retain their form under time-dependent conditions and, therefore, could be used as input in the momentum conservation equations. In a recent paper, we analysed the rheological response in time-dependent planar Couette flows using molecular dynamics simulations of a frictional granular packing [17]. It was found that the system evolves in two distinct phases. In the first one the non-local rheology describes accurately the system evolution, with similar values for the non-local correction as compared to Refs. [16, 18]. In the second phase the tempo-

⋆e-mail: rsoto@dfi.uchile.cl

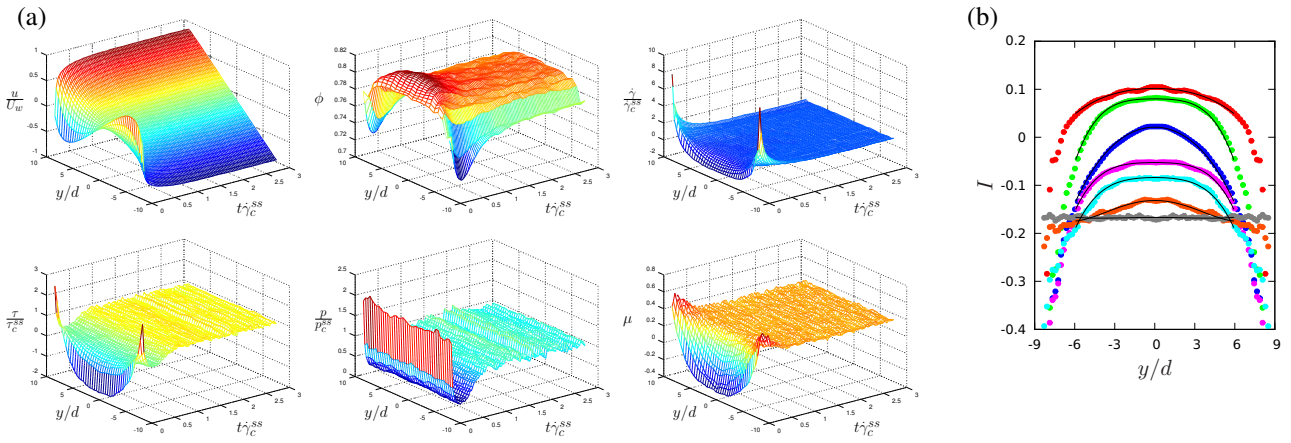

Figure 2. (a) Temporal evolution after the instantaneous velocity reversion from an initial (negative) steady shear, for $\phi_G = 0.790$ of the following fields: from left to right and top to bottom, horizontal velocity $u(x,t)$, volume fraction $\phi(y,t)$, shear rate $\dot\gamma(y,t)$, shear stress $\tau(y,t)$, pressure $p(y,t)$, and friction coefficient $\mu(y,t)$. Velocities are normalised to U_w and other field to the central value at the steady state. Colors, giving the field value, are used to enhance readability. (b) Vertical profile $I(y)$ for $\phi_G = 0.767$, at different instants of time (from top to bottom at $t\dot\gamma_c^{ss} = 0^+, 0.05, 0.25, 0.5, 1.0, 2.5, 5.0$). Solid lines are fits in the central region, used to compute $\kappa = d^2\nabla^2 I/I$.

ral evolution is characterised by the local rheology, even though the fluidity parameter does not vanish. Here, we present additional elements of this study.

2 Simulation method

The numerical set-up consists in a two dimensional dry granular medium confined between two rough walls in absence of gravity (see Fig. 1). The medium is made of a polydisperse mixture of circular grains with uniform mass density and diameters that are uniformly distributed in the range $[0.5d, 1.5d]$, where d is the average diameter and m_p is the average grain mass. The walls are made of similar particles, which will be forced to move at imposed velocities $\pm U_w$ to produce a planar Couette flow. The shear rate is $\dot\gamma_w = 2U_w/H$, H being the height of the flowing region. The system is periodic in the horizontal x direction, while it is limited by the walls in the vertical one. The horizontal size is $L = 45d$ and the system height is $H = 18d$. Finally, the wall thickness is $W = 1.5d$, such that all particles with their center in this region move together with the wall.

The granular model is the one used in Refs. [19] and [17]. The grains interact with visco-elastic forces in the normal and tangential directions, added to a tangential Coulomb friction, where the spring constant for the normal force is much larger than the maximal pressure reached in the simulations. Hence we remain in the hard particle limit for which the $\mu(I)$ rheology was obtained. Therefore, the microscopic dynamics is characterized by a unique time scale given by the shear rate, used to fix time units.

The initial configurations are prepared as follow. $N = 800$ particles are placed in the system between the walls. A fixed vertical pressure P_e is imposed on the walls to compress the system and a shearing motion is added until the system relaxes to the steady state. Depending on the imposed pressure, different global volume fractions ϕ^G between the walls are obtained in the range $0.767 < \phi^G < 0.805$, which is the only control parameter in our simulations. Having obtained the initial configurations, the wall separation is fixed and the following simulations are done *at constant volume*. Planar Couette flows are simulated with an imposed wall velocity U_w, until a stationary state is achieved. The stationary state is slightly inhomogeneous in the vertical direction (see Fig. 2) as a result of boundary effects, which have been shown to increase when decreasing the inertial number [20, 21]. Hence, we measure in the central region of the box (averaged over one third of the system height) the steady state volume fraction ϕ_c^{ss}, shear rate $\dot\gamma_c^{ss}$, pressure p_c^{ss}, and shear stress τ_c^{ss}. From these, the friction coefficient $\mu_c^{ss}$and inertial number I_c^{ss} in the centre are obtained. The friction coefficient is fitted to the standard expression $\mu_c^{ss} = \mu_1 + \frac{\mu_2-\mu_1}{1+I_0/I_c^{ss}}$ [1], where the fit parameters are $\mu_1 = 0.277$, $\mu_2 = 0.85$ and $I_0 = 0.364$, the same as those obtained in Ref. [22]. Also, the volume fraction and the inertial number in the central region are related in the usual form $\phi_c^{ss} = \phi^* - mI_c^{ss}$, with $\phi^* = 0.813$, as the extrapolated values for vanishing I_c^{ss}, and $m = 0.28$.

Transient regimes are obtained by instantly reversing the imposed velocities on the walls $\pm U_w$, where the sign alternates periodically. The alternation period is large allowing the system to reach a steady state before it is perturbed by the sudden change in shear direction. The process is repeated and averaged considering 1000 cycles. Here, we will analyse the relaxation process as a function of time, measured from the shear rate reversion.

3 System evolution

The relaxation process is strongly inhomogeneous temporally and spatially. Figure 2 displays the temporal evolution of all relevant fields, averaged over the horizontal direction x and the cycles, with time measure from the reversion instant: horizontal velocity $u(x,t)$, volume fraction $\phi(y,t)$, shear rate $\dot\gamma(y,t)$, shear stress $\tau(y,t)$, pres-

sure $p(y,t)$, friction coefficient $\mu(y,t)$, and inertial number $I(y,t)$. The shear rate and inertial number are obtained by fitting locally the velocity profile to low degree polynomials, to later derive them.

Throughout all the simulations we performed, we noticed that the system evolution can be characterized by two subsequent time phases, which can be simply visualized by inspection of the relaxation profiles. First, just after the shear reversion, large shear rates are produced near the walls as u changes from a linear Couette profile to the reverse one. These large shear rates heat up the granular medium, increasing globally the pressure. Associated to the large shear rates, there is an increase of pressure near the walls that push the system towards the centre, generating a transverse mass flux as shown by the vertical velocity v. This flux increases the density at the centre, which reaches a maximum at a characteristic time τ_1. Then, a second phase begins, where the density relaxes down to its steady state value. In this phase, the pressure field is spatially homogeneous and approaches its steady state value. Thus, the density relaxation is not driven any more by pressure gradients but qualitatively, by processes more akin to a diffusional relaxation, associated to non-affine motion. At all times, the corresponding shear rate fields $\dot{\gamma}(y,t)$ are spatially heterogeneous. The characteristic time of this phase is τ_2. Finally, both τ_1 and τ_2 scale with $1/\dot{\gamma}_c^{ss}$, however, the second phase lasts about ten times longer than the first phase. Also, no critical phenomena is observed when approaching ϕ^* [17].

4 Local and non-local rheology

Now we investigate the relations linking the dynamical friction coefficient and the packing fraction, to the inertial number. For this purpose we measure the volume fraction $\phi_c(t)$, inertial number $I_c(t)$, and friction coefficient $\mu_c(t)$ in the central region of the simulation box (averaged over one third of the system height). Figure 3 presents the system evolution of those variables in the μ-I and the ϕ-I spaces, for different global volume fractions ϕ_G. As a reference, in black, we display the relations $\mu(I)$ [Fig. 3(a)] and $\phi(I)$ [Fig. 3(b)] obtained in the central region for the stationary state. After the velocity reversal, the first phase corresponds to a strong departure from the $\mu(I)$ relation. However in the second phase, the relaxation to steady-state is taking place on the $\mu(I)$ curve. This final relaxation takes place either by increase or decrease of I_c according to the value of the global packing fraction ϕ_G.

For the packing fraction evolution [see on Fig. 3(b)], in no instance of the relaxation process, the local $\phi(I)$ relation is satisfied. Interestingly, the maximal ϕ_c value reached in the centre is always higher than the steady state value ϕ^* but still, I_c remains finite. In all cases, the volume fractions are smaller than the random close packing limit.

Figure 4 presents the temporal evolution of the central values of μ, ϕ, p and τ. It is remarkable the μ reaches the local rheology much before the pressure and the stress reach their steady values. That is, during the second phase p and τ continue to evolve, but they are not independent as

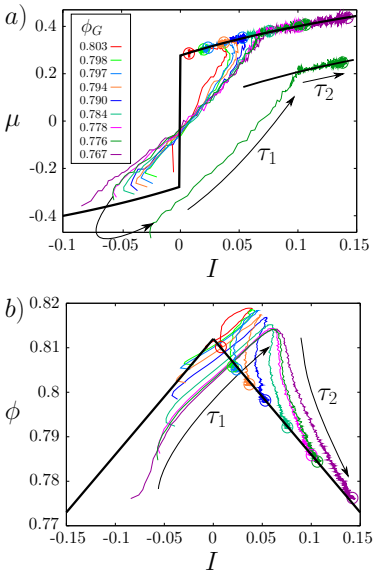

Figure 3. Temporal evolution (indicated by an arrow) of the system in the (a) μ-I, (b) ϕ-I spaces for quantities measured in the central region of the box. Different colours correspond to various global volume fractions ϕ_G. The black solid lines show the steady state relations $\mu(I)$ and $\phi(I)$ and the open circles show the final steady state values. To highlight the evolution in the two phases, for illustration purposes only, in the top figure we offset on both axis the relaxation curve for $\phi_G = 0.776$. First, during τ_1 the system does not follow the local rheology and the volume fraction increases until a maximum value is reached. In the second phase, of duration τ_2, the local rheology $\mu(I)$ is fulfilled but the volume fraction, which decreases monotonically while I increases, is not given by the steady state relation $\phi(I)$.

they are linked by the relation $\tau = \mu(I)p$. Finally, the volume fraction reaches steady state in a much longer scale.

To test the non-local rheology in the spirit of Bouzid *et al.* [16], we computed the parameter $\kappa = d^2\nabla^2 I/I$ associated with the local fluidity relative to the neighborhood. We obtain the second derivative of I in the centre, by fitting $I(y)$ by a fourth degree even polynomial (see Fig. 2). Figure 5(a) displays for $\phi_G = 0.767$ the time evolution of κ and one sees that it reaches zero after a time τ_1 but thereafter displays a rebound before reaching zero in the second part of the relaxation dynamics. Note that despite the boundary effects, which produce non-uniform shear rates [20, 21], the inertial number is almost uniform at the center in the steady state. Remarkably, when $\Delta\mu = \frac{\mu(I_c(t))-\mu_c(t)}{\mu(I_c(t))}$ is displayed as a function of κ [see Fig. 5(b)], one obtains a good collapse for the different volume fractions on a single curve $\chi(\kappa)$, hence validating the non-local relation as proposed by Bouzid *et al.* [16] of the type $\mu_c = \mu(I_c)\,[1-\chi(\kappa)]$. However for $t > \tau_1$, the non-local extension to the rheology is not valid. The departure in κ from zero is small but, systematic.

5 Summary and discussion

The relaxation process of a granular system in a planar Couette geometry at fixed volume is studied after the im-

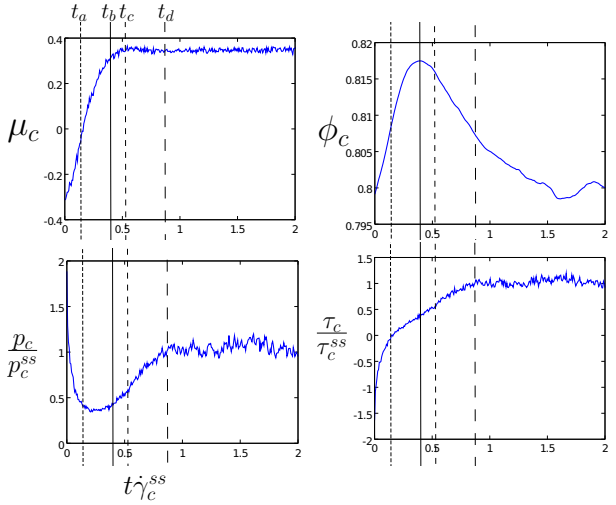

Figure 4. Temporal evolution of the central averaged value of μ, ϕ, p and τ, for $\phi_G = 0.790$. Different instants are represented by vertical lines. t_a: inertial number changes sign from negative to positive; t_b: maximum density is reached at the centre; t_c: μ_c reaches the local rheology value; and t_d: the shear stress reaches the steady value. For $t_c \leq t \leq t_d$, μ_c is not constant but evolves following the local rheology relation $\mu(I)$.

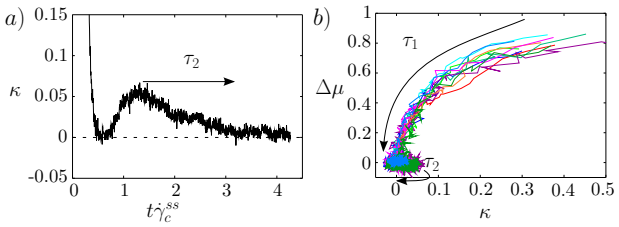

Figure 5. (a) Temporal evolution of the non-local parameter $\kappa = d^2\nabla^2 I/I$ at $\phi_G = 0.767$. Other volume fractions show similar behaviour, with smaller rebounds in κ when approaching ϕ_G^*. All quantities are evaluated at the center of the box. Time is measured from the instant of shear rate reversion. (b) $\Delta\mu$ plotted as a function of κ. Different colours correspond to the various simulated volume fractions (labels shown in Fig. 3).

posed shear rate is instantly reversed. We found that the system evolves in two phases. First, the steady local relation $\mu(I)$ is not satisfied but the measured value approaches exponentially the steady relation. In this phase the non-local rheology is satisfied with similar values for the non-local correction $\chi(\kappa)$ as compared to Refs. [16, 18]. Because of the pressure increase at the boundary there is a mass flux towards the centre of the cell such that density increases but the local constitutive relation $\phi(I)$ is not satisfied. Thereafter, there is a second phase where the system evolves following the local relation $\mu(I)$ found for steady flows. Finally, the time scales for both phases depend on the distance to the maximum packing fraction, but do not show any critical behaviour.

A salient result of this study is that κ is a good predictor for the non-local rheology observed in the first phase. However, in the second phase, where we identified smaller but systematic non-zero values for κ, the non-locality does not manifest itself in the $\mu(I)$ rheology. This observation points on the possibility of a relevant hidden variable accounting for non-locality. This variable would be similar to the fluidity parameter as defined by Bouzid *et al.* [16], but would relax faster to reach zero in the second phase.

This research is supported by Fondecyt Grant No. 1140778 and Ecos-Conicyt Grant C11E04. E.R. acknowledges the support of a Becas CONICYT. B.A. is supported by Institut Universitaire de France. This work is funded by the ANR JamVibe and a CNES research grant

References

[1] GDR MiDi, Eur. Phys. J. E **14**, 341 (2004).
[2] da Cruz F., Emam S., Prochnow M., Roux J. N., and Chevoir F., Phys. Rev. E **72**, 021309 (2005).
[3] Fortere Y. and Pouliquen O., Ann. Rev. of Fluid Mech. **40**, 1 (2008).
[4] O'Hern C. S., Langer S. A., Liu A. J., and Nagel S. R., Phys. Rev. Lett. **88**, 075507 (2002).
[5] Jop P., Forterre Y., and Pouliquen O., Nature **441**, 727 (2006).
[6] Cortet P.-P., Bonamy D., Daviaud F., Dauchot O., Dubrulle B., and Renouf M., EPL **88**, 14001 (2009).
[7] Weinhart T., Hartkamp R., Thornton A. R., and Luding S., Phys. Fluids **25**, 070605 (2013).
[8] Deboeuf S., Lajeunesse E., Dauchot O., and Andreotti B., Phys. Rev. Lett. **97**, 158303 (2006).
[9] Aranson I., Tsimring L.,t Malloggi F., and Clement E., Phys. Rev. E **72**, 031303 (2008).
[10] Komatsu T. S., Inagaki S., Nakagawa N., and Nasuno S., Phys. Rev. Lett. **86**, 1757 (2001).
[11] Nichol K., Zanin A., Bastien R., Wandersman E., and van Hecke M., Phys. Rev. Lett. **104**, 078302 (2010).
[12] Reddy K. A., Forterre Y., and Pouliquen O., Phys. Rev. Lett. **106**, 108301 (2011).
[13] Pouliquen O. and Fortere Y., Phil. Trans. R. Rol A **367**, 5091 (2009).
[14] Kamrin K. and Koval G., Phys. Rev. Lett. **108**, 178301 (2012).
[15] Henann D. L. and Kamrin K., Proc. Natl. Acad. Sci. USA **110**, 6730 (2013).
[16] Bouzid M., Trulsson M., Claudin P., Clement E., and Andreotti B., Phys. Rev. Lett. **111**, 238301 (2013).
[17] Rojas E., Trulsson M., Andreotti B., Clement E. and Soto R., EPL **109**, 64002 (2015).
[18] Bouzid M., Trulsson M., Claudin P., Clement E., and Andreotti B., EPL **109**, 24002 (2015).
[19] Luding S., Granular Matter **10**, 235 (2008).
[20] Miller T., Rognon P., Metzger B., and Einav I., Phys. Rev. Lett. **111**, 058002 (2013).
[21] Rognon P., Miller T., Metzger B., and Einav I., J. Fluid. Mech. **764**,171 (2014).
[22] Trulsson M., Andreotti B., and Claudin P., Phys. Rev. Lett. **109**, 118305 (2012).